J Mater Sci (2019) 54:9313–9320

Ceramics

Crystallization mechanism and kinetics of a Fe-diopside ($25CaO{\cdot}25MgO{\cdot}50SiO_2$) glass–ceramic

Valmor R. Mastelaro[1,*], Paulo S. Bayer[1,2], and Edgar D. Zanotto[3]

[1] São Carlos Institute of Physics, University of São Paulo, 13560-970 São Carlos, SP, Brazil
[2] Federal Institute of Santa Catarina, Campus Joinville, Joinville, SC CEP 89220-618, Brazil
[3] DEMa – CeRTEV – Federal University of São Carlos, Rodovia Washington Luis, Km. 235, São Carlos, SP 13.565-905, Brazil

Received: 14 December 2018
Accepted: 27 March 2019
Published online:
3 April 2019

© Springer Science+Business Media, LLC, part of Springer Nature 2019

ABSTRACT

Diopside-based ceramics and glass–ceramics have been studied because of their applications in electronics and biomedicine. However, since diopside glass presents poor internal nucleation ability, sintering combined with *surface crystallization* of powdered glasses has been reported to obtain diopside glass–ceramics. On the other hand, in this work, we explore the effect of an efficient nucleating agent (Fe_2O_3) to induce copious *internal* nucleation in this glass, which enabled the production of single-phase diopside glass–ceramics by the traditional route. The crystallization kinetics of a diopside glass ($25CaO{\cdot}25MgO{\cdot}50SiO_2$) containing 8.26 mol% of Fe_2O_3 was investigated under isothermal conditions by differential thermal analysis (DTA) and was modeled by the Johnson-Mehl-Avrami-Kolmogorov-Erofeev (JMAKE) equation. The crystals formed were iron-diopside—the X-ray diffraction pattern was indexed to the ferric-diopside card ($Ca_{0.991}(Mg_{0.641}Fe_{0.342})(Si_{1.6}Fe_{0.417})O_6$). Through a systematic DTA study, we successfully determined the mechanism and kinetics of crystallization of this material, which provided relevant information to guide the development of this novel type of internally crystallized glass–ceramic.

Introduction

Diopside ($25CaO{\cdot}25MgO{\cdot}50SiO_2$, hereafter denoted as CMS_2) is an important mineral of the pyroxene group, which presents a monoclinic structure of the C2/c4 space group [1, 2]. Partially or totally crystallized CMS_2-based materials have gained increased interest because of their potential applications as artificial bones, dental roots and crowns [3], as well as sealants for solid oxide fuel cells [4–6]. Such relevance can be associated with an adequate combination of high chemical durability, significant microwave dielectric properties and very high flexural strength (400 MPa) [7, 8]. However, diopside-based glass–ceramics (GC) containing different additives, such as La_2O_3, ZnO, B_2O_3, SrO and Cr_2O_3, present poor internal nucleation ability. For this reason, they have been mostly obtained by *sintering* with concurrent (surface) crystallization of glass powders,

Address correspondence to E-mail: valmor@ifsc.usp.br

https://doi.org/10.1007/s10853-019-03572-y

which often leads to residual porosity and other problems that are intrinsic to the sintering processes.

In principle, glass–ceramics can also be obtained from controlled internal crystallization of certain glasses. The process consists of forming a glass piece (e.g., by conventional melt-quenching method) and then submitting it to a heat treatment to induce internal nucleation and crystal growth [9–11]. The addition of nucleating agents, such as TiO_2, ZrO_2, P_2O_5, Cr_2O_3, Fe_2O_3, WO_3 and noble metals, is essential to foster the nucleation process in the interior of most glasses. Nevertheless, they are rather specific: Each glass composition demands a different nucleating agent [9–11], which is empirically found.

Only a few studies on the role of such catalyzers in diopside glass–ceramics have been published [3, 12, 13]. For example, Nonami and Tsutsumi [3] obtained $CaO–MgO–2SiO_2–0.375TiO_2–0.007Ag_2O$ glass–ceramic samples containing a small amount of diopside—between 15 and 25% (vol%)—as the only microcrystalline phase distributed in the glass. According to the authors, the brown color is a result of silver colloids inside the glass. Heat treatment at 870 °C induced the growth of such silver colloids and the subsequent precipitation of 1–2-μm diopside crystals, causing a whitish color. Despite the small amount of diopside, the bending strength of this glass–ceramic was surprisingly very high (400 MPa), making the material suitable for use as artificial bones. This result motivated us to study further and develop diopside glass–ceramics.

In the previous work, one of us [12] discovered the effect of Fe_2O_3 as a potential nucleating agent for diopside glass, although it was only superficially explored. In such a study, the authors analyzed the influence of Fe_2O_3 on the nucleation kinetics of $25CaO·25MgO·50SiO_2.xFe_2O_3$ glassy samples, with x equal to 3.9 and 7.9 mol%. In samples containing 7.9 mol% of Fe_2O_3, heat-treated at 720 °C for nucleation and subsequently at 940 °C for crystal growth, transmission electron microscope images showed the presence of nano-sized crystalline aggregates uniformly distributed throughout the specimen volume. These crystals could not be detected by X-ray diffraction because of their small sizes and low volume fraction. The authors suggested that they could be magnetite (Fe_3O_4). After a subsequent heat treatment at 800 °C for 2 h, they observed the presence of diopside crystals.

Recently, Zhang et al. [13] studied the effect of Cr_2O_3 on the crystallization kinetics of a diopside glass. They reported that the maximum achievable solubility of Cr_2O_3 in diopside was 3 wt%, and that a crystalline spinel phase was formed by the addition of 3 wt% $Cr_2O_3–MgCr_2O_4$—which acted as a nucleating agent for the diopside crystals.

In these previous studies, the crystallization kinetics of diopside glass containing a nucleating agent was not characterized. In addition, the properties of the resulting glass–ceramics were only cursorily described. However, the determination of the crystallization *mechanism* and *kinetics* may provide key information necessary for producing novel, optimized glass–ceramic materials via controlled internal crystallization. One method to do so is through *isothermal* treatments via DTA. Although a few studies have focused on this method to investigate the crystallization mechanism for inorganic glasses—by far, most authors often use non-isothermal DTA techniques [14, 15]. Thus, this study aims to determine the crystallization mechanism and kinetics, in a range of temperatures, of a diopside glass containing an efficient nucleating agent, Fe_2O_3.

Experimental details

Different amounts of Fe_2O_3 were tested; 6.54 and 8.26 mol% were enough to induce copious internal nucleation. However, in this article, we will focus on the 8.26 mol% composition for which we carried out a comprehensive study. To obtain the desired glass composition, 8.26 mol% of Fe_2O_3 was added exceeding 100 mol% of the stoichiometric $25CaO·25MgO·50SiO_2$ (CMS_2) diopside composition, which led to a $25CaO·25MgO·50SiO_2.8.26Fe_2O_3$ mol% composition, hereafter denoted as CMS_2-Fe.

To obtain vitreous samples of the CMS_2 and CMS_2-Fe, appropriate proportions of $CaCO_3$ (Alfa Aesar > 99.5%), MgO (Alfa Aesar, 99.95%), SiO_2 (Alfa Products, 99.9%) and Fe_2O_3 (Alfa Aesar 99.99%) were thoroughly mixed in a rotary mixer for 3 h. A 60-gram batch was melted in a platinum crucible at 1500 °C for 2 h, and then, plate samples were obtained by pouring the molten material in a thin metallic mold at room temperature. The melting process was followed by fast cooling between two metallic plates, and the procedure was repeated four times to promote homogenization. To relax the

thermal stresses arising from the non-uniform cooling process, the vitreous plates were submitted to an annealing treatment at 60 °C for 1 h below the respective glass transition temperatures.

The glass transition temperatures (T_g), the onset crystallization temperatures (T_c) and the peak crystallization temperature (T_p) of CMS_2 and CMS_2-Fe samples were determined through differential thermal analysis (DTA) measurements performed in air at a heating rate of 10 °C/min in a temperature range of 20 °C to 1100 °C using a 2910 Differential Thermal Analyzer from TA Instruments.

To verify the formation of crystals in the CMS_2-Fe glass volume, the sample underwent two subsequent heat treatments: first at 705 °C for 15 min and subsequently at 780 °C for 15 min. One side of the sample was polished by removing approximately 200 μm from its surface to reveal its internal crystals. The polished surface was then subjected to chemical etching in a 0.1% HCl–0.3% HF vol% for 15 s. Scanning electron micrographs and energy-dispersive X-ray spectra (EDX) of the samples were obtained in a Zeiss microscope model Sigma equipped with electron gun by field emission (SEM-FEG).

Determination of the temperature of maximum nucleation rate (T_{Nmax}) of the CMS_2-Fe sample

The temperature of maximum nucleation rate ($T_{Nmax.}$) of the CMS_2-Fe sample was determined by the DTA method proposed by Marotta et al. [16] using 30-mg pieces. The small monolithic pieces of vitreous samples were previously submitted to isothermal nucleation treatments in an electrical furnace at 645 °C, 655 °C, 665 °C, 675 °C, 685 °C, 695 °C and 705 °C for 2 h. These pre-nucleated samples were then subjected to DTA analysis using a heating rate of 10 °C/min to obtain the trace corresponding to each nucleation temperature. The temperature of maximum crystal nucleation rate (T_{Nmax}) corresponding to the maximum difference between $T_{p'}$ (DTA crystallization peak of the sample without pre-nucleation isothermal treatment) and T_p (DTA crystallization peak of a pre-nucleated vitreous sample) was then determined.

Isothermal crystallization mechanism and kinetics by DTA of the CMS_2-Fe sample

The *isothermal* crystallization method through DTA was used to determine the mass crystallized fraction (α) as a function of the treatment time and the Avrami coefficient (n), later described, of the CMS_2-Fe glass. The DTA measurements were performed using monolithic pieces of around 30 mg and a heating rate of 10 °C/min up to the isothermal treatment temperature. The time at the isothermal condition varied according to the temperature of study (760, 770, 780 and 790 °C). The experiments were interrupted after complete crystallization of each sample, that is, after the complete formation of the exothermic peak in the DTA trace as inferred by the return of the curve to its baseline.

Results and discussion

Figure 1 shows the DTA traces of a monolithic piece and a powdered sample (< 100 μm) of the CMS_2 and CMS_2-Fe glasses. From this figure, we determined the characteristic temperatures of each sample, which are presented in Table 1. As shown in that table, the addition of Fe_2O_3 led to a decrease in the T_g, T_c and

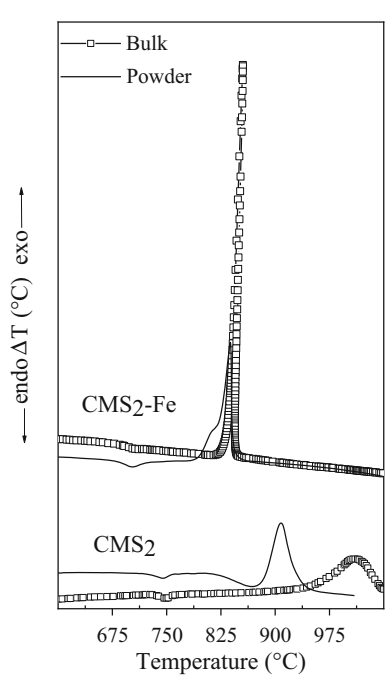

Figure 1 DTA traces of CMS_2 and CMS_2-Fe glassy samples in bulk and powder forms at a heating rate of 10 °C/min.

Table 1 Glass transition temperature, T_g, peak crystallization temperature, T_p, and onset crystallization temperature, T_c, of powdered and bulk samples. $\Delta T = T_c - T_g$

Sample	T_g (°C)	T_p (°C)	T_c (°C)	ΔT (°C)
CMS_2 bulk	731	1010	930	199
CMS_2 powder	731	908	870	139
CMS_2-Fe bulk	680	855	820	140
CMS_2-Fe powder	680	837	785	105

T_p and, consequently, of the value of ΔT in relation to the CMS_2 glass.

It is well established that the approximation of the crystallization peak temperatures of a powdered sample and the same material in monolithic form (ΔT_p) is an indication that the nucleation process happens predominantly in the sample interior [17]. Thus, a simple way of assessing whether internal nucleation is occurring is to verify the value of the ΔT_p. Whereas for the pure CMS_2 glass sample, which presents only surface nucleation, $\Delta T_p \approx 100$ °C, for the material containing Fe, $\Delta T_p \approx 18$ °C (Fig. 1). This result indicates that this amount of iron oxide added in the sample acted as an effective catalyzer for internal nucleation in diopside glass.

To prove that crystal nucleation really occurred in the glass interior, the sample was subjected to a heat treatment at 705 °C for 15 min (for nucleation) followed by another at 780 °C for 15 min to have its crystals revealed. As shown in Fig. 2, after the surface layer removal, multiple crystals could be observed in the sample cross section, indicating that the formation of crystals indeed occurred in the sample volume. To confirm that iron atoms were present in solid solution in the crystalline phase, an EDX analysis was made inside the crystal (square) and in the glass region (circle) (Fig. 2b). As shown in Fig. 2c, the EDX spectrum collected inside the crystal and in the glass region is quite similar, showing that Fe is indeed incorporated in the crystalline phase.

Figure 3 shows the X-ray diffraction pattern of a powdered glassy CMS_2 and CMS_2-Fe samples that underwent a crystallization treatment at the peak crystallization temperature (T_p) to induce (almost) full crystallization. We compared the XRD patterns of pure diopside (CMS_2) and iron-containing diopside glass (CMS_2-Fe) samples. From this comparison, we verified that the XRD patterns present significant differences, mainly in the 26–38 two-theta range. The diffraction pattern of the CMS_2 crystallized sample was indexed as diopside ($25CaO{\cdot}25MgO{\cdot}50SiO_2$, ICSD 30522 card). The XRD pattern of CMS_2-Fe sample that could only be fully indexed to the *ferric-diopside* phase ($Ca_{0.991}(Mg_{0.641}Fe_{0.342})(Si_{1.6}Fe_{0.417})O_6$, ICSD 85691 card) was considered. In this phase, Fe^{2+} ions can substitute Mg^{2+}, whereas Fe^{3+} can substitute Si^{4+} [1]. Mossbauer measurements (not shown) indicate that iron can be present as Fe^{+2} and Fe^{+3} in the original glass with a content of 16 and 84%, respectively.

Figure 4 shows the nucleation curve as a function of the temperature of nucleation treatment obtained by the method developed by Marotta [16] based on DTA data. The value of the temperature of maximum nucleation ($T_{Nmax.}$) is approximately 10 °C lower than T_g (682 °C). Although being rare to achieve a T_{Nmax} lower than T_g, this fact was also observed in a cordierite glass, which only exhibits internal nucleation as a result of the addition of a large amount of TiO_2 [18].

Crystallization kinetics of the CMS_2-Fe glass by the isothermal DTA method

The kinetics of isothermal crystallization can be described based on a theory developed by Johnson and Mehl, Avrami, Kolmogorov and Erofeev, known as JMAKE phase transformation theory [19]. They proposed the following equation for general use:

$$\alpha_v(t) = 1 - exp\,(-Kt^n) \quad (1)$$

where $\alpha_v(t)$ is the *volume* fraction transformed; ***n*** is the Avrami coefficient, a numerical factor related to the nucleation mechanism and growth morphology of crystals; and the coefficient K is related to the crystal shape, nucleation and growth rates.

Equation (1) can be linearized, resulting in the following logarithmic form:

$$ln\,(-ln\,(1 - \alpha_v)) = lnK + nlnt \quad (2)$$

The isothermal DTA method consists of heating a glass sample at a constant rate in the DTA equipment up to the desired temperature of isothermal treatment and maintaining it at that temperature during the exothermic crystallization transition, i.e., from the beginning to the end of crystallization peak. Figure 5a shows the normalized DTA crystallization peaks as a function of time between 760 and 790 °C for the CMS_2-Fe glass. The results indicate a single,

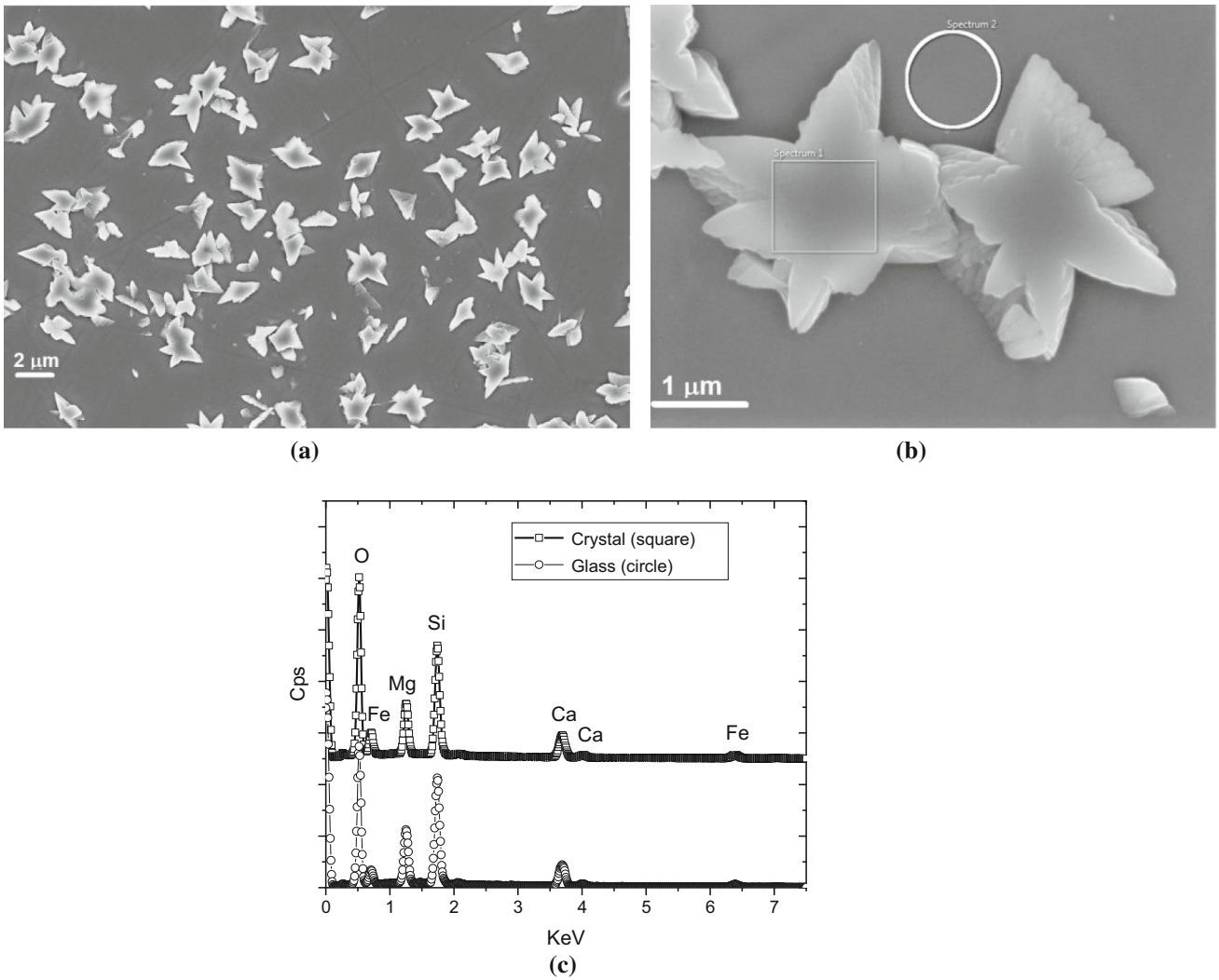

Figure 2 Electron micrograph of the cross section of a CMS_2–9Fe glass sample heat-treated at 705 °C/15 min for nucleation and subsequently at 780 °C/15 min for crystal development. **a** Small (< 5 µm) crystals are uniformly distributed in the sample interior. **b** SEM micrograph showing details where the EDX analysis was performed. **c** EDX spectra obtained inside the crystal (square) and in the glass region (circle).

smooth process of isothermal crystallization with the formation of ferric-diopside. The exothermic crystallization peaks of the ferric-diopside phase shift to lower temperatures and become narrower and more intense, confirming the expected progressive increase in the crystallization rate as the temperature of the isothermal treatment increases.

The typical experimental points of the sigmoidal curves represent a variation in the crystallized mass fraction, α_m, as a function of time, t, for the different isothermal temperatures. They were inferred from the crystallization peak areas. The crystallized mass fraction can be calculated as follows [20, 21]:

$$\alpha_m = A_t/A \tag{3}$$

where (A_t) is the partial area of the peak at the time t and (A) is the total area of the peak, as indicated in the inset of Fig. 5a.

The data obtained by isothermal heating in the DTA equipment refer to the crystallized mass fraction (α_m). However, to interpret these data through JMAKE equation, it is necessary to convert them into a volumetric crystallized fraction (α_v), according to the following Eq. (4):

$$\alpha_v = \frac{\alpha_m \rho_g}{\rho_c - (\rho_c - \rho_g)\alpha_m}, \tag{4}$$

where α_v and α_m are the crystallized volume and mass fractions, respectively, being ρ_g = 2.87 g/cm^3

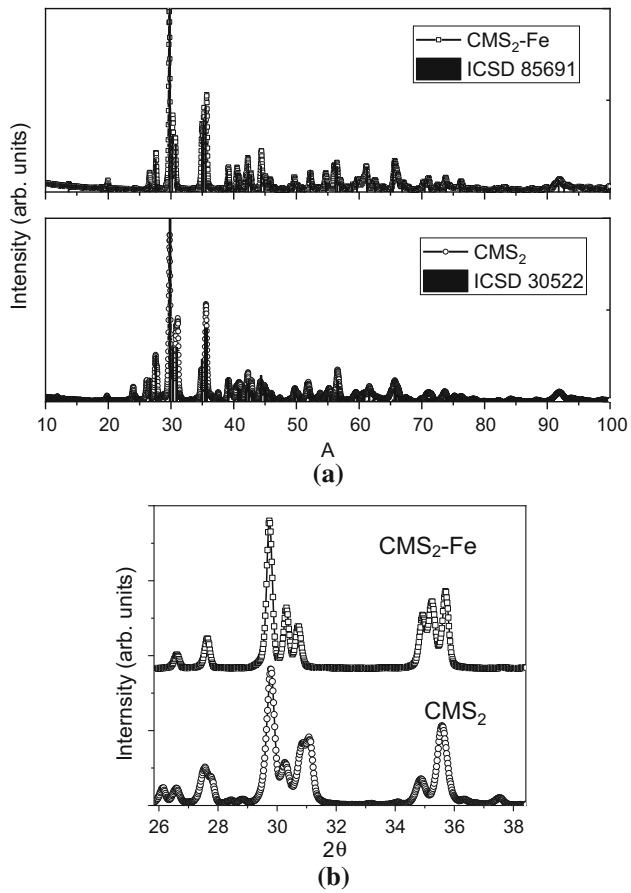

Figure 3 X-ray diffraction patterns of the crystallized CMS_2 and CMS_2-Fe glassy samples: **a** CMS_2 X-ray diffraction pattern indexed to the ICSD File 30522 ($25CaO{\cdot}25MgO{\cdot}50SiO_2$ phase) and CMS_2-Fe X-ray diffraction pattern indexed to the 85691 ICSD File ($Ca_{0.991}(Mg_{0.641}Fe_{0.342})(Si_{1.6}Fe_{0.417})O_6$ phase). **b** Comparison of the XRD patterns of CMS_2 and CMS_2-Fe samples showing the 2θ range where the differences are more significant).

and $\rho_c = 3.27\ g/cm^3$, the reported values for the diopside glass and crystal densities, respectively.

The experimental points in Fig. 5b formed sigmoidal curves of crystallized mass fraction (α_m) and crystallized volume fraction (α_v) as a function of time, t, for different temperatures. The density difference (13%) causes differences between the two data sets. As expected, the time necessary for full crystallization decreases as the temperature increases from 760 °C to 790 °C.

Once the time dependence of crystallized volume fraction during isothermal annealing experiments is obtained, the Avrami coefficient, $\boldsymbol{n}$, can be determined by the slope of the graph $\ln(-\ln(1-\alpha_v))$ versus $\ln t$ (Eq. 2). According to the literature, n can

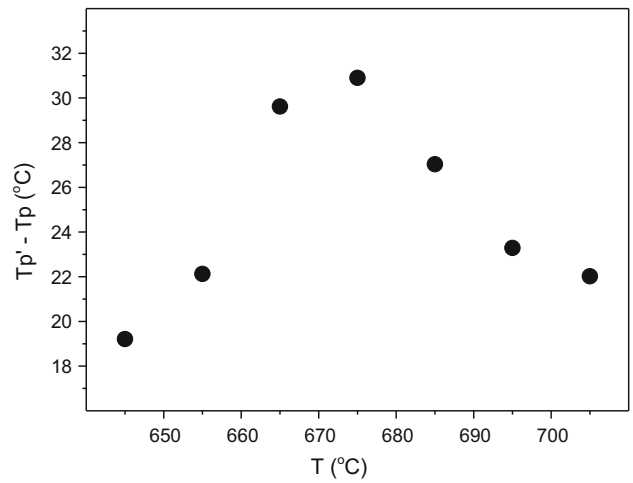

Figure 4 Plot of $T_{p'}$–T_p *versus* temperature of nucleation treatment. T_p corresponds to the peak crystallization temperature in the DTA trace of monolithic pieces previously submitted to nucleation treatments at different temperatures for 2 h. $T_{p'}$ is the crystallization peak in the DTA curve of the as-obtained glassy sample.

vary from 0.5 to 4.0 depending on the crystallization mechanism and crystal morphology [22].

To determine the Avrami coefficient, the experimental α_v curves were used. Graphs of $\ln[-\ln(1-\alpha_v)]$ versus $\ln(t)$ resulting from the crystallization isotherms at 790, 780, 770 and 760 °C are shown in Fig. 6. According to the previous studies, for $0 < \alpha < 0.1$, the $\ln[-\ln(1-\alpha_v)]$ values are strongly affected by small variations in α_v, since it is difficult to determine an exact measure of the area under the crystallization peak at the beginning, which may consequently lead to incorrect values. In addition, the final stages of crystallization ($\alpha_v \sim 0.8$) can also cause measurement difficulties and curvature in the linearized graphs [23, 24]. To minimize such possible problems, only values corresponding to the crystallized volume fraction range ($0.3 < \alpha_v < 0.7$) were used to estimate the value of n [23, 24]. The results shown in Fig. 6 were determined by least squares fitting of the experimental data in this interval and correspond to the line slopes.

This procedure resulted in an average value of $n = 3.2 \pm 0.3$. Considering that the median value of n is very close to **3**, the mechanism of crystal growth for the CMS_2-Fe glass can be interpreted as interface-controlled crystal growth from a fixed number of nuclei during the isothermal crystallization process in the DTA [22]. This value of n is approximately temperature independent. Consequently, the CMS_2-Fe

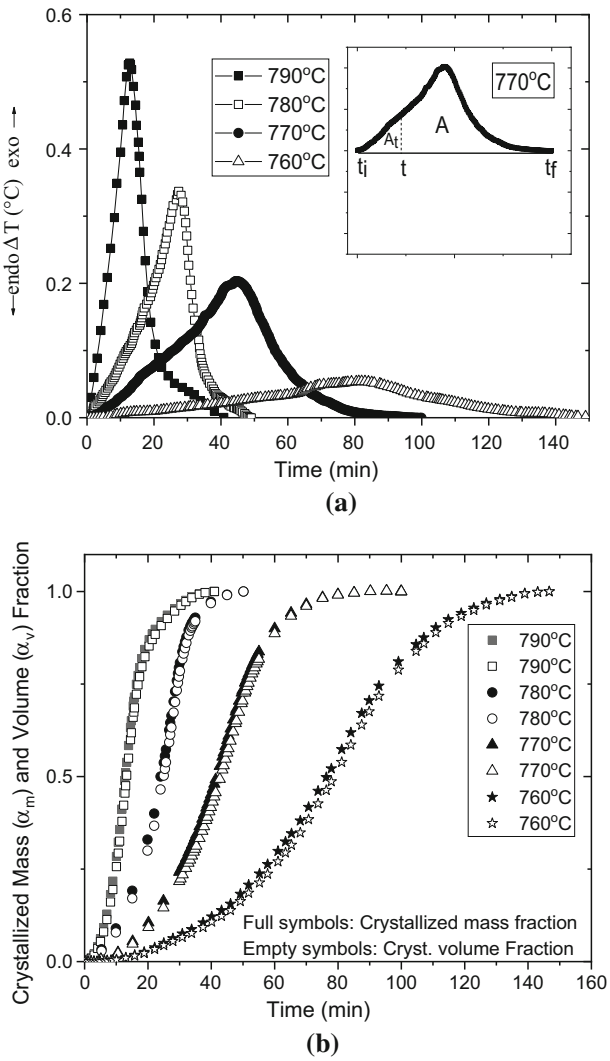

Figure 5 **a** Time dependence of the DTA signal during isothermal annealing of CMS_2-Fe glassy samples at 760 °C, 770 °C, 780 °C and 790 °C. **b** Time dependence of the crystallized mass fraction (α_m) and crystallized volume fraction (α_v) during isothermal annealing of CMS_2-Fe glassy samples at 760 °C, 770 °C, 780 °C and 790 °C.

glass undergoes internal nucleation, which occurs during the heating path in the DTA, when the sample temperature crosses the nucleation peak at 670–680 °C, independent of the chosen (final) crystallization temperature.

This value of $n \sim 3$ clearly indicates the growth of three-dimensional crystals from a constant number of nucleation sites in the sample interior. We have not discovered the nature of the nucleation sites yet. However, the crystal nuclei were clearly formed on the heating path, crossing the nucleation curve

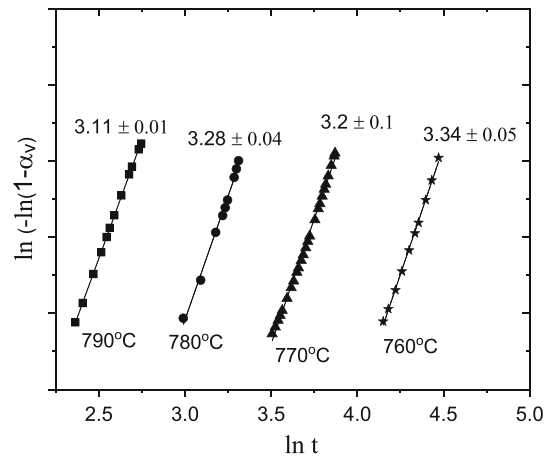

Figure 6 Ln[(− ln(1 − α_v)] versus ln t (logarithm of time) plots for the isothermal crystallization of the CMS_2-Fe glass at four temperatures well above the T_{Nmax}. The continuous lines resulted from linear fittings of the experimental data at each temperature. The numbers above the lines refer to the Avrami coefficients.

maximum at 672 °C and reaching temperatures from 760 to 790 °C (Fig. 6).

As seen in the above results, through specific thermal treatments it is possible to produce microstructured diopside glass–ceramics. This study could be extended into four fronts: (1) to determine the chemical mechanism of nucleation; (2) to characterize the properties of the current glass–ceramics; (3) to add a little more Fe_2O_3 to further boost the nucleation rates; or (4) to increase the treatment time at the temperature of maximum nucleation to develop nano-structured glass–ceramics (nano-GC). Such nano-GC could perhaps show interesting, unusual properties.

Conclusions

We induced copious internal nucleation in a diopside glass by adding enough Fe_2O_3, which enabled the production of microstructured diopside glass–ceramics. We then studied the crystallization mechanism and kinetics of such promising material. The value of the Avrami exponent $n \sim 3$ indicates the growth of tridimensionally shaped crystals from a fixed number of internal nucleation sites. Taken *in toto*, these results are relevant and could guide the development of novel diopside glass–ceramics.

Acknowledgements

We are thankful to the São Paulo Research Foundation (FAPESP) for funding this research, under the grant number 2013/07793-6 (CEPID). P.S. Bayer would also like to thank the Federal Institute of Science, Technology and Education of Santa Catarina for granting him a leave of absence to complete his doctoral studies.

Compliance with ethical standards

Conflict of interest All the authors declare that they have no conflict of interest.

References

[1] Redhammer GJ (1998) Mössbauer spectroscopy and rietveld refinement on synthetic ferri-Tschermak's molecule $CaFe^{3+}(Fe^{3+}Si)O_6$ substituted diopside. Eur J Mineral 10:439–452

[2] Morimoto N (1988) Nomenclature of pyroxenes. Miner Pet 39:55–76

[3] Nonami T, Tsutsumi S (2000) Press-formable CaO-MgO-SiO_2-TiO_2-Ag_2O glass as a biomaterial. J Biomed Mater Res 50:8–15

[4] Goel A, Tulyaganov Du, Pascual MJ et al (2010) Development and performance of diopside based glass-ceramic sealants for solid oxide fuel cells. J Non Cryst Solids 356:1070–1080

[5] Reddy AA, Tulyaganov DU, Mather GC et al (2014) Effect of strontium-to-calcium ratio on the structure, crystallization behavior and functional properties of diopside-based glasses. Int J Hydrog Energy 39:3552–3563

[6] Reddy AA, Tulyaganov DU, Kharton VV, Ferreira JMF (2015) Development of bilayer glass-ceramic SOFC sealants via optimizing the chemical composition of glasses—a review. J Solid State Electrochem 19:2899–2916

[7] Chou CC, Feng KC, Raevski IP et al (2017) Part I: effects of two-stage heat treatment on densification, microstructural features and dielectric properties of CaO–MgO–SiO_2 glass-ceramics with ZrO_2 nucleating agents. Mater Res Bull 96:66–70

[8] Feng KC, Chou CC, Chu LW, Chen H (2012) Zirconia nucleating agent on microstructural and electrical properties of a $CaMgSi_2O_6$ diopside glass-ceramic for microwave dielectrics. Mater Res Bull 47:2851–2855

[9] Zanotto ED (2011) A bright future for glass ceramics. Am Ceram Soc Bull 89:609–612

[10] Davis MJ, Zanotto ED (2017) Glass-ceramics and realization of the unobtainable: property combinations that push the envelope. MRS Bull 42:195–199

[11] Deubener J, Allix M, Davis MJ et al (2018) Updated the definition of glass-ceramics. J Non Cryst Solids 501:3–10

[12] Colombrini R, Zanotto ED, Craievich AF (1981) Vitrocerâmicos a partir de materias primas naturais. Ceramica 27:213–218

[13] Zhang S, Zhang Y, Wu T (2018) Effect of Cr_2O_3 on the crystallization behavior of synthetic diopside and characterization of Cr-doped diopside glass ceramics. Ceram Int 44:10119–10129

[14] Ray CS, Zhang T, Reis ST, Brow RK (2007) Determining kinetic parameters for isothermal crystallization of glasses. J Am Ceram Soc 90:769–773

[15] Zhang T, Brow RK, Reis ST, Ray CS (2008) Isothermal crystallization of a solid oxide fuel cell sealing glass by differential thermal analysis. J Am Ceram Soc 91:3235–3239

[16] Marotta A, Buri A, Branda F (1981) Nucleation in glass and differential thermal analysis. J Mater Sci 16:341–344

[17] Donald IW (1995) The crystallization kinetics of a glass based on the cordierite composition studied by DTA and DSC. J Mater Sci 30:904–915

[18] Fokin VM, Zanotto ED (1999) Surface and volume nucleation and growth in TiO_2-cordierite glasses. J Non Cryst Solids 246:115–127

[19] Fokin VM, Zanotto ED, Yuritsyn NS, Schmelzer JWP (2006) Homogeneous crystal nucleation in silicate glasses: a 40 years perspective. J Non Cryst Solids 352:2681–2714

[20] Prasad NS, Varma KBR (2005) Crystallization kinetics of the $LiBO_2$–Nb_2O_5 glass using differential thermal analysis. J Am Ceram Soc 88:357–361

[21] Choi HW, Kim YH, Rim YH, Yang YS (2013) Crystallization kinetics of lithium niobate glass: determination of the Johnson-Mehl-Avrami-Kolmogorov parameters. Phys Chem Chem Phys 15:9940–9946

[22] Christian JW (1965) The theory of transformations in metals and alloys: an advanced textbook in physical metallurgy, vol 1, 1st edn. Pergamon Press, Oxford

[23] Bansal NP, Doremus RH, Bruce AJ, Moynihan CT (1983) Kinetics of crystallization of ZrF_4-Ba_2-LaF_3 glass by differential scanning calorimetry. J Am Ceram Soc 66:233–238

[24] Pietrzak TK, Wasiucionek M, Nowiński JL, Garbarczyk JE (2013) Isothermal nanocrystallization of vanadate-phosphate glasses. Solid State Ionics 251:78–82

Publisher's Note Springer Nature remains neutral with regard to jurisdictional claims in published maps and institutional affiliations.